Particle Accelerators, 1995, Vol. 49, pp. 253–271
Reprints available directly from the publisher
Photocopying permitted by license only

ANALYTICAL DESCRIPTION OF PARTICLE MOTION IN RADIO-FREQUENCY PHOTO-INJECTORS

LUCA SERAFINI

INFN and Università di Milano
Via Celoria 16 – 20133 Milano, Italy

(Received 9 June 1994; in final form 25 January 1995)

In this paper the analytical expressions are derived for the particle trajectory and beam envelope of photo-electrons generated by a laser pulse on a photocathode inside a Radio-Frequency linear accelerator.

The particle motion is described taking into account the fast transition, due to rapid acceleration by the high gradient RF field, from non-relativistic motion, close to the cathode surface, up to relativistic velocities (typically at a few MeV kinetic energy) at the accelerator exit.

Both RF and space charge effects are taken into account in calculating the beam dynamics: the moments of the transverse phase space distribution, as predicted at the accelerator exit, agree quite remarkably with the results of sophisticated particle-in-cell simulations. The results apply almost to any kind of RF cavity geometry, since the accelerating field is specified simply by giving its spatial-harmonic content. The model applies to medium-high gradient injectors with moderate bunch charge: its validity range can be summarized as $E_0[MV/m] \gtrapprox 10 \cdot \nu_{\mathrm{RF}}[GHz]$, and $Q[nC] \lessapprox \frac{E_0[MV/m]}{10}$, where ν_{RF} is the RF frequency of the accelerator, E_0 is the peak field at the cathode and Q the bunch charge.

Most of the treatment used in this paper can be eventually applied to describe other phenomena related to electron emission inside high gradient accelerating structure (e.g. dark currents, field emission, etc.).

KEY WORDS: Injectors, linear accelerators, particle dynamics

1 INTRODUCTION

Theoretical investigations of electron beam dynamics in RF photo-injectors[1,2] has been addressed in the past by many authors,[3–15] with special aim to find a general optimization of the whole system (RF cavity geometry, frequency and gradient, laser pulse format, solenoid lenses, etc.), in view of achieving the maximum beam brightness as to fulfill the tight requirements typical of future linac-based Free Electron Lasers in the X-UV domain and/or electron-positron colliders in the TeV energy range.

For both applications intense electron beams are required with very low emittance and low energy spread, in order to meet either the high-gain operation requirements of an FEL or the luminosity specifications of a TeV collider.

A common assumption of previous analytical studies[3,6,7,12] was the invariance of the beam envelope through the first cells of the RF injector cavity: the main beam quantities

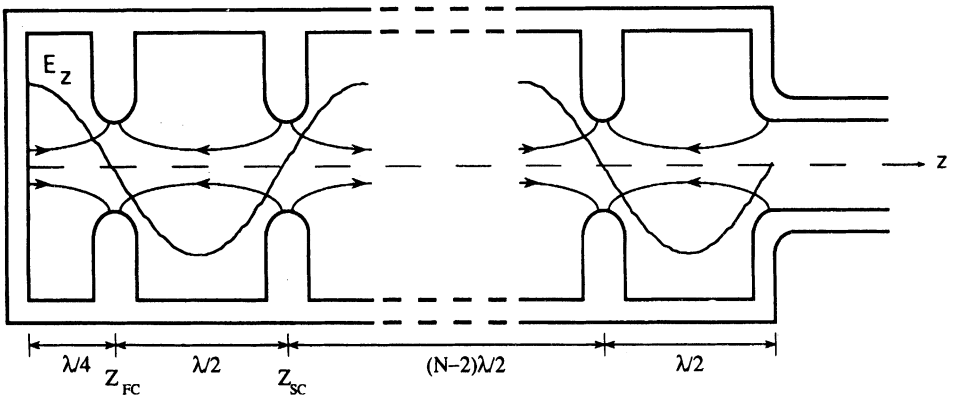

FIGURE 1: Schematic cross section in the (r,z) plane of a typical RF multi-cell cavity of a photo-injector gun: the RF field distribution on-axis is plotted together with the electric field lines of the $TM_{010-\pi}$ mode in use for electron acceleration. The cathode is located at z=0.

(rms transverse and longitudinal emittance, rms divergence, rms energy spread, etc.) were computed assuming a straight line trajectory at constant radius, $r = r_0$, for electrons emerging at radius r_0 from the cathode surface and accelerated up to the gun exit. Only in Ref. 4 the beam envelope was specified *a priori* by a quadratic form corresponding to a nearly-constant space charge force, neglecting however the focusing-defocusing RF effects.

In this paper we show how to describe analytically the behavior of the rms beam envelope through the gun, under the effect of both RF and space charge fields. Formulae for the particle position r and momentum p_r at the exit of the first one and half cells are given, together with the rms beam size σ_r and divergence σ_r' of a gaussian charged bunch. The dynamics in the following cells of the RF injector cavity, where the beam has become relativistic, is described again analytically using the RF transport matrix recently derived,[15] which is able to reproduce quite accurately the beam envelope as predicted by sophisticated and time consuming numerical simulations.

A typical RF multi-cell cavity used for RF photo-injectors is drawn in Figure 1, displaying the cross section of an axi-symmetric iris-loaded structure terminated into a half cell hosting the cathode (located at $z = 0$) and operated in a $TM_{010-\pi}$ standing mode with $\lambda/2$ cells. The general expression of the RF field components expanded linearly off-axis is:[13]

$$\begin{cases} E_z = \varepsilon_z(r,z)\cdot\sin(\omega t+\varphi_0)\ ;\ \varepsilon_z(r,z) = E_0 \sum\limits_{n=1,\text{odd}}^{\infty} a_n \cos(nkz) \\ E_r = \varepsilon_r(r,z)\cdot\sin(\omega t+\varphi_0)\ ;\ \varepsilon_r(r,z) = \frac{kr}{2}E_0 \sum\limits_{n=1,\text{odd}}^{\infty} n\cdot a_n \sin(nkz)\ ; \quad a_1 = 1 \\ B_\theta = B_\theta(r,z)\cdot\cos(\omega t+\varphi_0)\ ;\ B_\theta(r,z) = c\frac{kr}{2}\varepsilon_z(r,z) \end{cases} \tag{1}$$

where $k \equiv 2\pi/\lambda = \omega/c$, and a_n are the spatial harmonic coefficients which depends on the actual cavity geometry: they can be easily computed by RF eigenvalue-finder codes

(Superfish, MAFIA, etc.) or derived by experimental bead measurements. Due to the symmetry of the selected mode, all even a_n's are vanishing; since $a_1 = 1E_0$ becomes the amplitude of the fundamental harmonic component in the RF wave. All higher harmonic amplitudes are therefore normalized to the fundamental one.

The RF transverse force F_r acting on a relativistic particle of charge e, traveling at $v_z = c$ close to the symmetry axis (i.e. at $kr \ll 1$) is given by[7,15]:

$$F_r = -eE_0\frac{kr}{4}\sum_{n=1,\text{odd}}^{\infty}(n+1)\{a_n\cos[(n+1)kz+\varphi_0] - a_{n+2}\cos[(n+1)kz-\varphi_0]\} \quad (2)$$

where the substitution $\omega t = kz$ is understood. It is instructive to look at the first harmonic component of the RF transverse force, $F_{r,n=1} = -eE_0\frac{kr}{2}\cos(2kz+\varphi_0)$, because it clearly shows that the $TM_{010-\pi}$ RF wave is seen by the particle as a series of focusing-defocusing lenses at a frequency doubled than ω: each half cell in the linear accelerating structure corresponds to one of these lenses.

In Section 2 the single particle transverse dynamics is analyzed in order to derive an expression for the trajectory. Basic steps followed are in order:

- by using the impulsive approximation[9] we assume that photoelectrons are emitted from the cathode at the speed of light, but at a phase φ shifted from the injection phase φ_0 and equal to the exit phase from the RF field.
- applying Panofsky-Wenzel theorem[16] as shown elsewhere[11] we calculate the first order transverse kick p_r^I imparted by RF field at the exit of the first half cell and of the second cell.
- the exit radii r_1 at the first half cell ($z = z_{FC}$) and r_2 at the second one ($z = z_{SC}$) are evaluated assuming that p_r^I is adiabatically distributed along the acceleration from the cathode throughout the two cells.
- the final transverse imparted momentum p_r is given at $z = z_{SC}$ by superimposing the contribution coming from the second-order ponderomotive RF focusing force.[15]
- starting from the derived (r_2, p_r) conditions at the exit of the second cell, where the beam has typically a kinetic energy of a few MeV, the trajectory can be generated quite accurately using the recently derived[15] transport matrix for multi-cell linear accelerating structures

Collective dynamics, dealing with space charge force effects, is described in Section 3. These are actually taken into account by evaluating *a la Kim*[3] the transverse kick generated by the space charge field close to the cathode, and averaging over the transverse phase space distribution to obtain the rms space charge transverse momentum. Main aim is to achieve an analytical prediction of the beam envelope in the photo-injector: the evaluation of the space charge emittance growth gives of course same results as Kim's formulae. As shown by comparisons to PIC simulations, the validity of the whole approach (RF + space charge) is surprisingly good when the dimensionless parameter[3] $\alpha \equiv \frac{eE_0}{2mc^2k}$, characterizing the RF field strength (m is the electron rest mass), is larger than $\frac{1}{2}$ and the bunch charge

Q (expressed in nC) is lower than $\frac{E_0}{10}$ (in MV/m): the operating range of most RF photo injectors in operation or under project is well contained within these specifications, so that the results derived in this paper are well applicable to a wide range of such devices.

2 SINGLE PARTICLE DYNAMICS IN RF MULTI-CELL GUNS

It has already been shown elsewhere[9] that the longitudinal dynamics can be treated very simply by assuming that photo-electrons are quickly accelerated by the strong RF field applied at the cathode surface and brought to relativistic velocities in a distance short with respect to the RF wavelength λ.

The RF field during this short time can be approximated by a DC field of amplitude $\mu \cdot E_0 \sin\varphi_0$, where μ is defined as $\mu \equiv \sum_{n=1}^{\infty} a_n$, so that the electron motion in the longitudinal direction is simply given by $z = ct - \frac{1}{2\mu(\alpha k)\sin\varphi_0}$; this corresponds to assume that electrons are emitted at the speed of light from the cathode surface, at a phase φ shifted with respect to the actual injection phase φ_0, according to

$$\varphi = \varphi_0 + \frac{1}{2(\mu\alpha)\sin\varphi} \tag{3}$$

so that the energy γ comes out to be $\gamma = 1 + \alpha(kz)\sin\varphi + \alpha \cdot \sin(kz)\sin(kz + \varphi)$.[17] Defining γ_1 and γ_2 as the normalized electron energies at the exit of the first half cell and of the second cell, respectively, we have:

$$\gamma_1 = 1 + \frac{\pi\alpha}{2}\sin\varphi + \alpha \cdot \cos\varphi\ ; \quad \gamma_2 = 1 + \frac{3\pi\alpha}{2}\sin\varphi + \alpha \cdot \cos\varphi \tag{4}$$

As shown later on, the phase $\varphi = \pi/2$ is of particular interest because it corresponds to the minimum transverse emittance: in Figure 2 we show a comparison between the analytical prediction of Eq. 3 evaluated at this phase, i.e. $\varphi_{0m} = \pi/2 - 1/(2\alpha)$, and a systematic of numerical calculations performed at different RF frequencies and field amplitudes (all cases with a pure first harmonic field, $\mu = 1$). The agreement, quite good at higher α, becomes somewhat poor at $\alpha < 1.5$: the numerical fit shown by the dashed curve (at $\varphi = \pi/2$),

$$\varphi_0 = \varphi - \frac{1}{2(\mu\alpha)\sin\varphi} - \frac{1}{10(\mu\alpha)^2\sin^2\varphi} \tag{5}$$

can be used to link the injection phase to the exit phase φ, in terms of which all the expressions following in this paper will be given. Other fits to link φ_0 to φ have been proposed,[10] especially to reproduce the low α range ($\alpha < 0.5$).

The predicted energy γ_2 at the exit of the second cell, for the case $\varphi = \pi/2$, is plotted (solid line) in Figure 3 and compared to the same numerical calculation set of Figure 2: this is actually the phase of maximum energy gain in the cells following the gun, where the beam is relativistic and synchronous to the RF wave. Dashed line corresponds to a phase φ shifted by 20° RF above $\pi/2$: the agreement is quite good (within 0.5%) in both cases.

Now we proceed to calculate the first order transverse momentum p_r^I, which is defined as the kick induced by the RF force F_r (Eq. 2) on a particle travelling along a straight trajectory

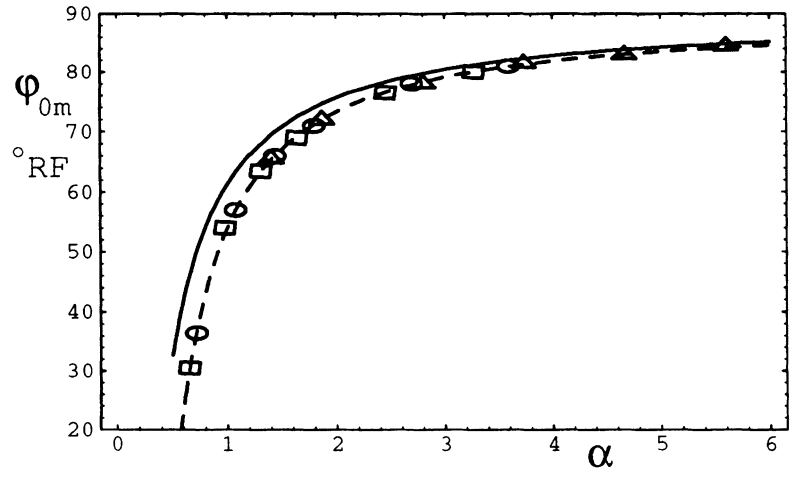

FIGURE 2: Injection phase φ_{0m} at the cathode corresponding to an exit phase $\varphi=\pi/2$, plotted as a function of α. The solid line corresponds to the analytical formula of Eq. (3) (with $\mu=1$), dashed line gives the numerical fit of Eq. (5). Symbols are numerical integration results corresponding to different RF frequencies and fields: 500 MHz (triangle), 1.3 GHz (circle), 2.856 GHz (square).

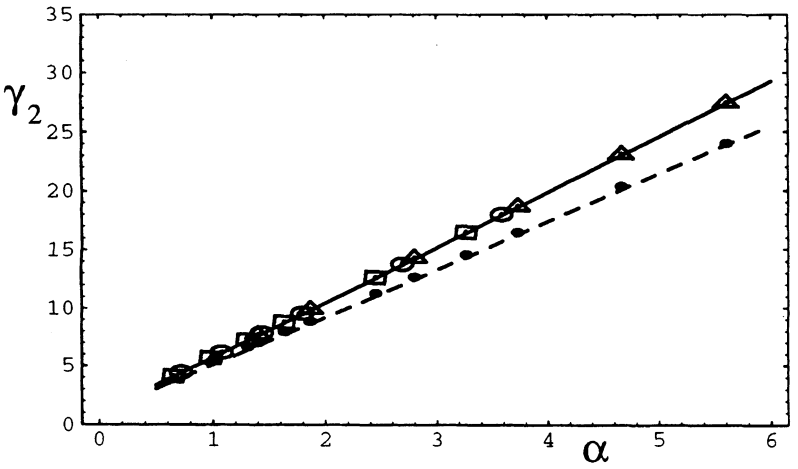

FIGURE 3: Normalized energy γ_2 at the exit of the second cell ($z=z_{SC}$) as a function of α. The solid line gives maximum energy gain at $\varphi=\pi/2$, while dashed line corresponds to $\varphi=(\pi/2+\pi/9)$.

at $r = r_0$. By calculating $p_r^I = \frac{1}{mc}\int_0^{(N+1/2)\lambda/2} F_r dt$, where N is the number of full cells in the structure (all momenta are taken dimensionless), we find

$$p_r^I = \alpha(kr_0)\mu \cdot \sin\varphi \tag{6}$$

after substituting φ_0 with φ in Eq. 2, according to the impulsive approximation. It is interesting to notice that this result can be obtained[11] applying Panofsky-Wenzel theorem[16] to the RF photo injector cavity , and that Eq. 6 is a generalization of a previous result[3] to RF fields containing higher harmonics.

Since p_r^I does not display any dependence on the number of cell N, we can imagine that the transverse kick is adiabatically transferred from the field to the particle, so that an approximation to the trajectory will be $r = r_0 + \frac{1}{z}\int_0^z \frac{z' p_r^I}{\gamma} dz'$. In order to simplify the integral we take into account only the linear average increase in γ, i.e. we put $\overline{\gamma}$, defined as $\overline{\gamma} \equiv 1 + \alpha(kz)\sin\varphi$, instead of γ inside the integral. The exit radius $\bar{r}_1$ at the first and $\bar{r}_2$ at the second cell become:

$$\bar{r}_1 = r_0\left\{1 + \mu\left\{1 - \frac{\log(\overline{\gamma}_1)}{\overline{\gamma}_1 - 1}\right\}\right\}\ ; \quad \bar{r}_2 = r_0\left\{1 + \mu\left\{1 - \frac{\log(\overline{\gamma}_2)}{\overline{\gamma}_2 - 1}\right\}\right\} \tag{7}$$

with $\overline{\gamma}_1 \equiv 1 + \frac{\pi\alpha}{2}\sin\varphi$, and $\overline{\gamma}_2 \equiv 1 + \frac{3\pi\alpha}{2}\sin\varphi$.

It is worthwhile to note that the trajectory depends only on the dimensionless parameter α and the phase φ, besides the harmonic content of the field given by μ. For the case $\varphi = \pi/2$ and $\mu = 1$ we plot in Figure 4 a comparison between Eq. 7 and numerical calculations related to the same RF field parameter set of previous figures. As clearly visible, the exit radius at the second cell, $\bar{r}_2$, is in agreement within 1% with numerical data all over the range $0.5 < \alpha < 6$.

In order to evaluate the total transverse momentum imparted by the RF force we must take into account the actual shape of the trajectory $r = r(z)$ and substitute it into Eq. 2. Following Ref. 15, we find that particles are subject to a RF ponderomotive gradient K_r given by $K_r = \frac{\alpha^2 k^2}{8\gamma^2}\eta$, where $\eta \equiv \sum_{n=1}^{\infty}(a_{n-1}^2 + a_{n+1}^2 - 2a_{n-1}a_n + 1\cos(2\phi))(a_0 \equiv 0)$. This gives rise to a second order focusing force $\overline{F}_r = -mc^2\gamma K_r \cdot \bar{r}$, which applies to the average (secular) component of the trajectory. Its effect, in terms of the transverse momentum, is taken into account assuming an average radius $\bar{r}$ for the trajectory equal to $\bar{r} = (\bar{r}_1 + \bar{r}_2)/2$. The negative transverse kick $\Delta\overline{p}_r$ generated by such a ponderomotive force is therefore given by

$$\Delta\overline{p}_r = -\frac{\alpha^2 k^2 \eta}{16}(\bar{r}_1 + \bar{r}_2)\int_0^{z_{SC}} \frac{dz}{\overline{\gamma}}$$

which in turn, added to the first order term p_r^I, generates the total transverse momentum p_r at the exit of the second cell

$$p_r = \alpha k \cdot \sin\varphi\left[\mu \cdot \bar{r}_1 - \delta\frac{\eta \log\overline{\gamma}_2}{16\sin^2\varphi}(\bar{r}_1 + \bar{r}_2)\right] \tag{8}$$

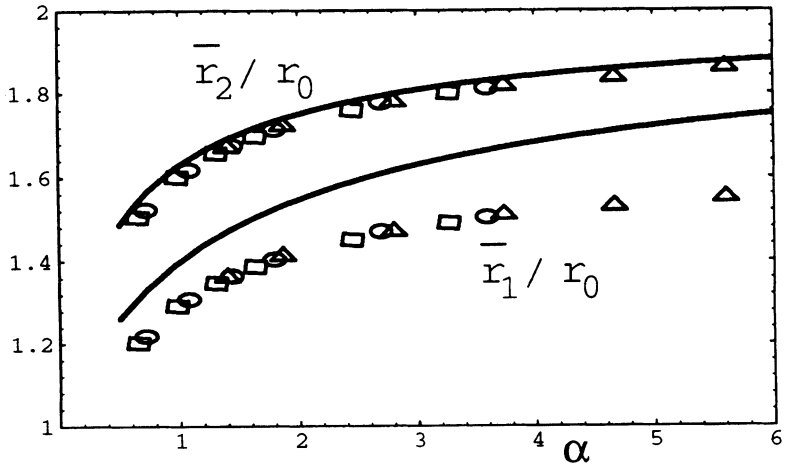

FIGURE 4: Exit radius $\bar{r}_1$ (lower curve) at the first cell ($z=z_{FC}$) and $\bar{r}_2$ (upper curve) at the second cell ($z=z_{SC}$, Eq. 7), normalized to the starting radius r_0 at the cathode surface ($\varphi=\pi/2$ and $\mu=1$).

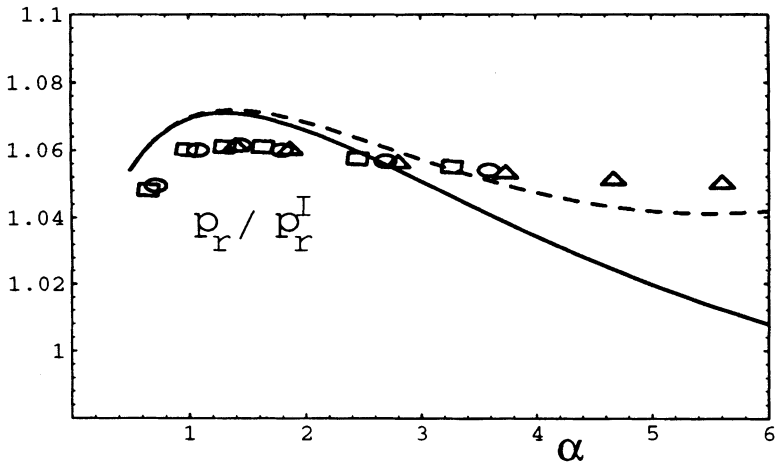

FIGURE 5: Exit transverse momentum p_r at the second cell ($z=z_{SC}$, Eq. 8), normalized to the first order kick p_r^I (Eq. 6), at $\varphi=\pi/2$ and $\mu=1$: solid line is with $\delta=1$, while dashed corresponds to $\delta=1-(\alpha/4!)^2$.

This is plotted in Figure 5 (solid line) as a function of α, for $\varphi = \pi/2$ and $\mu = 1$. The curves correspond actually to the quantity (p_r/p_r^I) (p_r^I is in this case $p_r^I = \alpha k r_0$), which is used for comparison to previous evaluations,[3,6,7,11] whose predictions were simply $p_r/p_r^I = 1$. In order to improve the agreement with the data at higher α's, we found that a small correction factor δ, defined as $\delta \equiv 1 - (\alpha/4!)^2$, is adequate to guarantee an agreement within 1% in the range $0.5 < \alpha < 6$. Let us remind that $\alpha = 6$ actually represents an upper bound to the present state of the art in the RF photo injector technology: indeed, it corresponds to a 65 MV/m peak field E_0 at a frequency of 500 MHz or 170 MV/m at 1.3 GHz. On the other side, only X-band injectors above 10 GHz may stay below $\alpha < 0.5$. One should however note that the CEA photoinjector,[12] operated at $\alpha = 9$ (144 MHz, 28 MV/m), is the only special case not included in the description of this model, due to the particular geometry of the RF gun cavity.

Real multi-cell structures for RF photo injectors usually have small higher space harmonic content,[13,18] in order to avoid emittance dilution due to non linear RF effects. We checked the analytical predictions of Eqs. 7 and 8 versus numerical data obtained by integrating particle motion inside a RF field, as specified by Eq. 1, either with a negative third harmonic coefficient $a_3 = -0.1$ (i.e. a slightly flat-topped field, $\mu = 0.9$, all other harmonic amplitudes are zero) or with $a_3 = +0.1$ (i.e. a field with enhanced peak value at the cathode surface, $\mu = 1.1$). The results are reported in Figure 6 and Figure 7 for the exit radius r_2 and transverse momentum p_r, respectively, for $\varphi = \pi/2$ (triangles for $a_3 = -0.1$, squares for $a_3 = 0$ and circles for $a_3 = +0.1$). The flat-topped field displays a lower radius and momentum, as already known[6,9]: the agreement is again quite good, within a few percent of the worst case.

In order to be able to evaluate accurately the transverse emittance growth due to linear RF effects, we must test preliminary the phase dependence of exit radius and momentum: since Eq. 7 has been derived substituting γ with $\overline{\gamma}$, to find a better expression for r_2 we repeat the calculation taking now $\gamma = 1 + \alpha(kz)\sin\varphi + \alpha\cos\varphi$, that seems a better approximation. In this way r_2 becomes

$$r_2 = r_0 \left\{ 1 + \mu \left[1 - (1 + \alpha\cos\varphi) \frac{\log \gamma_2}{\gamma_2 - 1 - \alpha\cos\varphi} \right] \right\} \tag{9}$$

Its behavior as a function of α is plotted in Figure 8, for two values of φ, $\varphi = \pi/2 \pm \pi/18$, while the phase dependence of the momentum p_r is shown in Figure 9, again in terms of the quantity (p_r/p_r^I) (where p_r^I is intended to be $p_r^I\ (\varphi = \pi/2) = \alpha k r_0$).

The normalized rms transverse emittance ε_x is defined for an axi-symmetric beam in terms of the moments of the transverse phase space distribution, i.e. $\varepsilon_x \equiv \frac{1}{2}\sqrt{< r^2 >< p_r^2 > - < r p_r >^2 + < r^2 >< p_\theta^2 >}$, where $< y >$ means an average of the quantity $y = y(r, p_r, \Delta\varphi, \Delta p_z)$ over the whole 4-D phase space distribution.[3,12] Usually the term $< p_\theta^2 >$ is negligible as far as no external magnetic focusing from a solenoid is applied: it keeps the cathode temperature contribution to the azimuthal momentum p_g, which is fairly negligible with respect to the radial momentum p_r.

We will assume that electrons are distributed inside the bunch according to a gaussian both

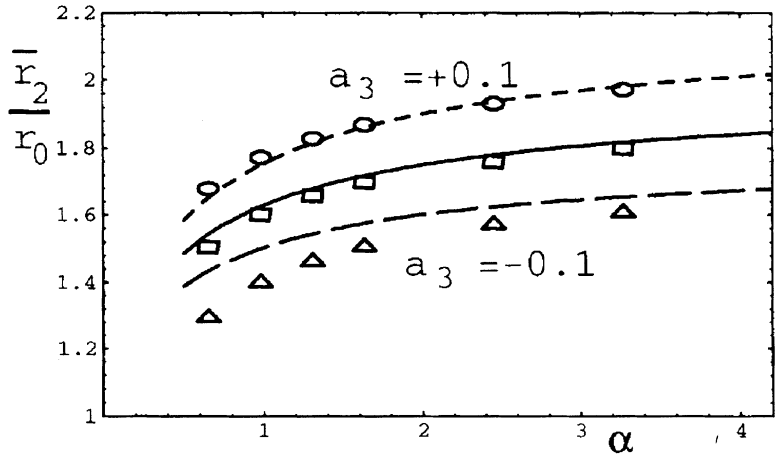

FIGURE 6: Exit radius $\bar{r}_2$, divided by the starting radius r_0, for three different values of the third harmonic coefficent a_3: triangles $a_3 = -0.1$, squares $a_3 = 0$, circles $a_3 = +0.1$.

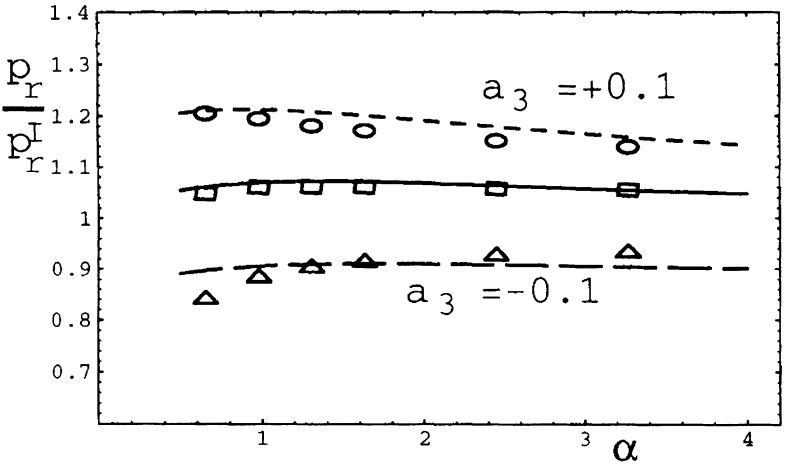

FIGURE 7: Exit momentum p_r (Eq. 8), divided by p_r^I, for three different values of the third harmonic coefficent a_3: triangles $a_3 = -0.1$, squares $a_3 = 0$, circles $a_3 = +0.1$.

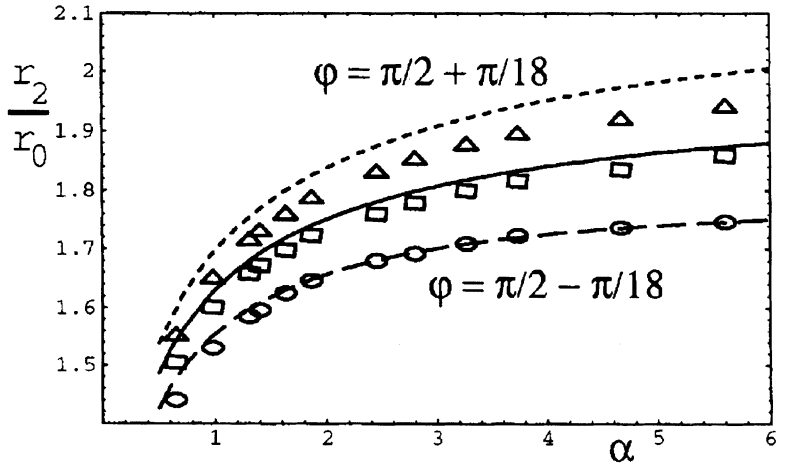

FIGURE 8: Exit radius r_2 (Eq. 9), divided by the starting radius r_0, for three different values of the exit phase φ: circles $\varphi=\pi/2-\pi/18$, squares $\varphi=\pi/2$, triangles $\varphi=\pi/2+\pi/18$.

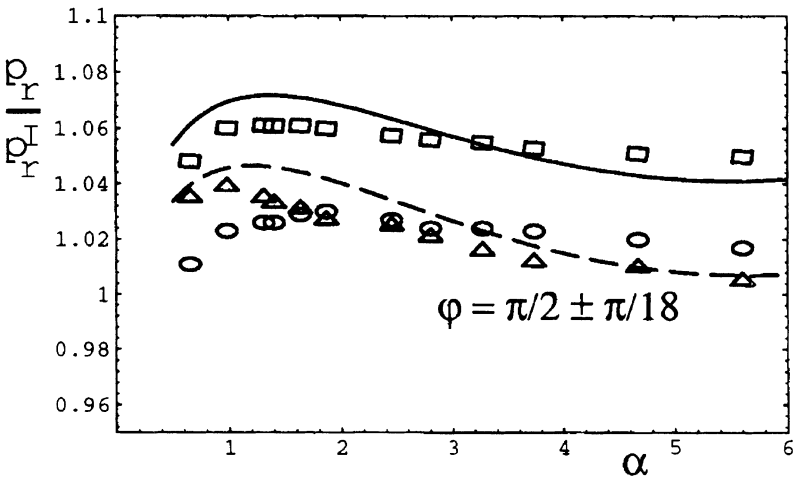

FIGURE 9: Exit radius momentum p_r (Eq. 8), divided by p_r^I, for three different phases φ: circles $\varphi=\pi/2-\pi/18$, squares $\varphi=\pi/2$, triangles $\varphi=\pi/2+\pi/18$.

in radius and in phase, so that the charge density ρ is defined as $\rho \equiv \frac{Qk}{2\pi\sqrt{2\pi}\sigma_r^2\sigma_\varphi} \exp(-\frac{r^2}{2\sigma_r^2} - \frac{\Delta\varphi^2}{2\sigma_\varphi^2})$, where $\Delta\varphi \equiv \varphi - <\varphi>$ and σ_r is the beam envelope starting at σ_0 on the cathode (σ_0 is actually the gaussian width of the laser pulse and $\sigma_\varphi \equiv k\sigma_z$ its length). Recalling that $<r^2> = 2\sigma_r^2$ and $<p_r^2> = 2\sigma_{pr}^2$ for a cylindrical beam, we re-define the emittance ε_x as

$$\varepsilon_x \equiv \sqrt{\sigma_r^2\sigma_{pr}^2 - <rp_r>^2/4} \tag{10}$$

In order to compute σ_r and σ_{pr} we must average $r_2(\varphi)$ and $p_r(\varphi)$ (Eq. 9 and 8, respectively) over the phase distribution in the bunch, i.e.

$$\sigma_r^2 = \frac{\sigma_0^2}{\sqrt{2\pi}\sigma_\varphi r_0^2} \int_{-\infty}^{+\infty} \exp\left(-\frac{\Delta\varphi^2}{2\sigma_\varphi^2}\right) r_2^2(\varphi) d(\Delta\varphi) \tag{11}$$

$$\sigma_{pr}^2 = \frac{\sigma_0^2}{\sqrt{2\pi}\sigma_\varphi r_0^2} \int_{-\infty}^{+\infty} \exp\left(-\frac{\Delta\varphi^2}{2\sigma_\varphi^2}\right) p_r^2(\varphi) d(\Delta\varphi) \tag{11'}$$

$$<rp_r> = \frac{\sigma_0^2}{\sqrt{2\pi}\sigma_\varphi r_0^2} \int_{-\infty}^{+\infty} \exp\left(-\frac{\Delta\varphi^2}{2\sigma_\varphi^2}\right) r_2(\varphi) p_r(\varphi) d(\Delta\varphi) \tag{11''}$$

After developing $r_2(\varphi)$ and $p_r(\varphi)$ in Taylor series up to second order in φ around $<\varphi>$, and substituting in Eq. 11, 11′ and 11″, we find expressions for σ_r, σ_{pr} and $<rp_r>$ in terms of σ_0, σ_φ, α, μ, η and $<\varphi>$. Substituting these quantities into Eq. 10, the emittance ε_x is obtained as a function of the RF field characteristics (α, μ, η), bunch sizes (σ_0 and σ_φ) and the average bunch phase $<\varphi>$: ε_x represents in this case the emittance growth caused by linear RF effects. For the case of a typical set of parameters, $\nu_{RF} = 500$ MHz, $E_0 = 25$ MV/m (i.e. $\alpha = 2.34$, $\mu = \eta = 1$), $\sigma_0 = 2$ mm, $\sigma_\varphi = 7.2°$RF (40 ps), we plot in Figure 10 the behavior of ε_x as a function of $<\varphi>$ (solid line), compared to numerical data obtained by the multi-particle code ITACA[19] (dots), and to the previous analytical expression[3] ε_k for the RF emittance growth (dashed line), $\varepsilon_k \equiv \alpha k\sigma_0^2(\frac{\sigma_\varphi^2}{\sqrt{2}} + \sigma_\varphi \cos <\varphi>)$.

Since the quantity of real interest is the minimum value of ε_x as a function of $<\varphi>$, it is worthwhile to report here only the involved expressions evaluated at $<\varphi> = \pi/2$: this is again (as in Ref. 3) the phase where ε_x displays a minimum, as shown in Figure 10.

First of all we need to define some needed quantities $\hat{\gamma}_1$, $\hat{\gamma}_2$, $\hat{\delta}_1$, $\hat{\delta}_2$, $\hat{\varepsilon}_1$, $\hat{\varepsilon}_2$, $\hat{r}_1$, $\hat{r}_2$, $\hat{p}_r$, $\hat{\varepsilon}_k$, which are the expressions assumed at $<\varphi> = \pi/2$ by some quantities defined above:

$$\hat{\gamma}_1 \equiv 1 + \frac{\pi\alpha}{2}, \hat{\gamma}_2 \equiv 1 + \frac{3\pi\alpha}{2}, \hat{\delta}_1 \equiv 1 - 2\frac{\log\hat{\gamma}_1}{\pi\alpha}, \hat{\delta}_2 \equiv 1 - 2\frac{\log\hat{\gamma}_2}{3\pi\alpha},$$

$$\hat{\varepsilon}_1 \equiv \frac{1}{\hat{\gamma}_1} - 2\frac{\log\hat{\gamma}_1}{3\pi\alpha}, \hat{\varepsilon}_2 \equiv \frac{1}{\hat{\gamma}_2} - 2\frac{\log\hat{\gamma}_2}{3\pi\alpha}, \hat{r}_1 \equiv 1 + \mu\hat{\delta}_1, \hat{r}_2 \equiv 1 + \mu\hat{\delta}_2$$

$$\hat{p}_r \equiv \mu\hat{r}_1 - \delta\frac{\eta\log\hat{\gamma}_2}{16}\left(2 + \mu(\hat{\delta}_1 + \hat{\delta}_2)\right), \hat{\varepsilon}_k \equiv \alpha k\sigma_0^2\frac{\sigma_\varphi^2}{\sqrt{2}}.$$

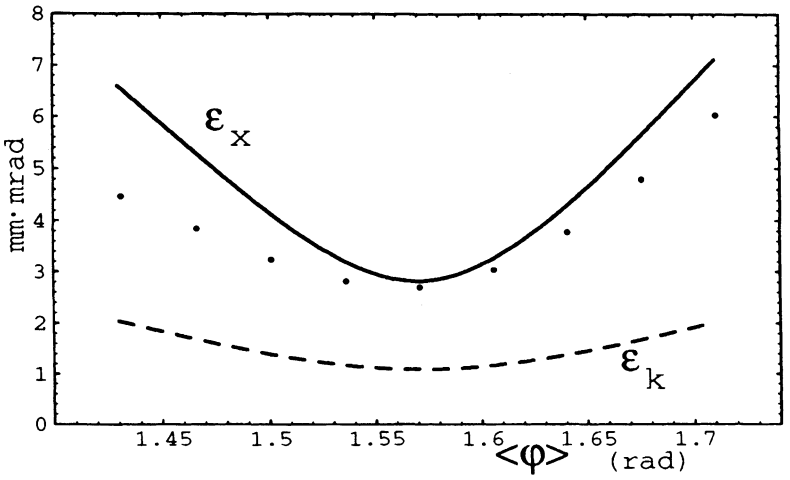

FIGURE 10: Rms normalized transverse emittance growth ε_x due to linear RF effects, plotted as a function of the average bunch phase $<\varphi>$ (solid line), compared to ε_k (dashed line) and to numerical data (dots). Field and beam parameters are: ν_{RF} = 500 MHz, E_0 = 25 MV/m, σ_0 = 2 mm, σ_φ = 7.2°RF (40 ps).

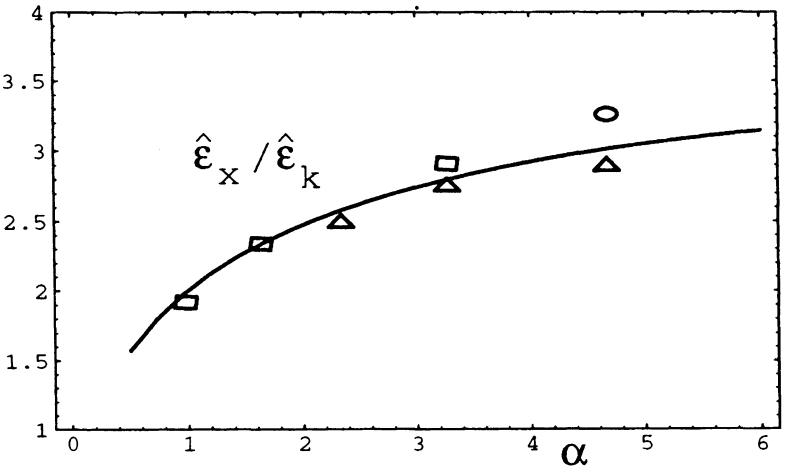

FIGURE 11: Minimum emittance $\hat{\varepsilon}_x$ (at $<\varphi>=\pi/2$), plotted (solid line, Eq. 14) as a function of α, expressed in units of $\hat{\varepsilon}_k$. The numerical data are: squares, ν_{RF} = 2.856 GHz (E_0 = 50, 100, 200 MV/m) σ_0 = 0.5 mm σ_φ = 5.1°RF (5 ps), triangles, ν_{RF} = 500 MHz (E_0 = 25, 35, 50 MV/m) σ_0 = 2 mm σ_φ = 7.2°RF (40 ps), circle, ν_{RF} = 500 MHz (E_0 = 50 MV/m) σ_0 = 0.5 mm σ_φ = 1.8°RF (10 ps).

These are functions of only α, μ and η, i.e. of the RF field characteristics, except for $\hat{\varepsilon}_k$, which is the minimum emittance growth calculated in Ref. 3. The rms beam transverse size σ_r (at $z = z_{sc}$) comes out to be

$$\sigma_r = \sigma_0 \left\{ (1 + \mu\hat{\delta}_2) + \right. \tag{12}$$

$$\left. + \frac{\mu\sigma_\varphi^2}{2(\hat{\gamma}_2 - 1)} \left[\log\hat{\gamma}_2 - \frac{(\hat{\gamma}_2 - 1)}{\hat{\gamma}_2} + \alpha^2 \frac{2\hat{\gamma}_2 - 1}{\hat{\gamma}_2^2} - \frac{\mu\alpha^2(1/\hat{\gamma}_2 + \log\hat{\gamma}_2)}{(\hat{\gamma}_2 - 1)(1 + \mu) - \mu\log\hat{\gamma}_2} \right] \right\}$$

and the rms transverse momentum σ_{pr}

$$\sigma_{pr} = \alpha \cdot k\sigma_0 \left\{ \hat{p}_r - \frac{\sigma_\varphi^2}{2} \left[\hat{p}_r - \mu^2\hat{\epsilon}_1 - \right. \right. \tag{13}$$

$$\left. \left. - \delta\frac{\eta \log\hat{\gamma}_2}{16} \left(\mu\left(\hat{\epsilon}_1 + \hat{\epsilon}_2\right) - \left(\mu\left(\hat{\delta}_1 + \hat{\delta}_2\right) + 2 \right) \left(\frac{\hat{\gamma}_2 - 1}{\hat{\gamma}_2 \log\hat{\gamma}_2} - 2 \right) \right) \right] \right\}$$

It is worthwhile to compare these quantities with previous evaluations,[3] that gave $\sigma_r = \sigma_0$ and $\sigma_{pr} = \alpha k\sigma_0(1 - \sigma_\varphi^2/2)$. The dependence of σ_r on σ_φ is actually very weak: we verified indeed that the coefficient of σ_φ^2 in Eq. 11 is quite negligible, so that an expression of σ_r for practical applications (i.e. when $\sigma_\varphi < 25°$RF) is

$$\sigma_r = \sigma_0(1 + \mu\hat{\delta}_2) \tag{12'}$$

This is due mainly to the fact that r_2 (at constant α) has a quasi-linear behavior versus φ around $\varphi = \pi/2$, as well displayed in Figure 8: when the average bunch phase $< \varphi >$ is equal to $\pi/2$ the bunch head (located at φ lower than $\pi/2$) has a smaller transverse size than the bunch tail, in such a way that the whole rms bunch size σ_r is almost unaffected with respect to the size of the bunch central slice, located at $\varphi = \pi/2$.

Substituting Eq. 12 and 13 into the definition of ε_x, Eq. 10, we get an expression for the minimum emittance growth $\hat{\varepsilon}_x$ at $< \varphi >= \pi/2$:

$$\hat{\varepsilon}_x = \frac{\hat{\varepsilon}_k \cdot \hat{r}_2}{\sqrt{2}} \left\{ \begin{array}{l} 2(\mu\hat{r}_1 - \hat{p}_r) - \mu\left(1 + \mu\frac{\hat{\gamma}_1 - 1}{\hat{\gamma}_1}\right) + \\ +\delta\frac{\eta}{16}\left[2\log\hat{\gamma}_2 \left(\mu\frac{\hat{\gamma}_2 - \hat{\gamma}_1}{\hat{\gamma}_1\hat{\gamma}_2} - 2\mu - 1 \right) + (\hat{r}_1 + \hat{r}_2)\frac{\hat{\gamma}_2 - 1}{\hat{\gamma}_2} \right] \end{array} \right\} \tag{14}$$

A plot of the quantity $(\hat{\varepsilon}_x/\hat{\varepsilon}_k)$ is drawn in Figure 11 (solid line) and compared to some numerical data obtained on a representative sample of different RF field and bunch parameter sets. Note that numerical results are weakly spread around the solid line, with a quite small effect due to the RF frequency (triangle dots versus square dots, i.e. 500 MHz vs. 2.856 GHz) and a larger but still moderate effect related to the bunch shape (triangle versus circle at $\alpha = 4.67$, i.e. $\{\sigma_0 = 2$ mm, $\sigma_z = 12$ mm, $\hat{\varepsilon}_k = 2.18$ mm.mrad$\}$ vs. $\{\sigma_0 = 0.5$ mm, $\sigma_z = 3$ mm, $\hat{\varepsilon}_k = 0.0085$ mm.mrad$\}$, respectively).

In order to produce simplified expressions for the quantities of interest, namely σ_r, σ_{pr} and $\hat{\varepsilon}_x$, we performed a fit over α, μ and η of the coefficients containing such parameters in Eq. 12, 13 and 14. Final approximated expressions are reported in the last section, where a synopsis of the analytic formulae is presented.

3 COLLECTIVE PARTICLE DYNAMICS IN RF MULTI-CELL GUNS

The basic model used to evaluate space charge effects is the same as in Ref. 3, where it is assumed that the total transverse momentum change p_r^{sc}, induced by space charge field throughout the acceleration, is given by:

$$p_r^{sc} = \frac{\pi}{2E_0 \sin\phi_0} E_r^{sc} \tag{15}$$

stating that p_r^{sc} is proportional to the radial component of the electrostatic field E_r^{sc} produced by the bunch charge at rest in the laboratory frame, divided by the actual RF field at the cathode surface $E_0 \sin\phi_0$, at the time the bunch is emitted from the cathode.

For a gaussian charge distribution in the bunch, as the one defined above, E_r^{sc} is given by[20]

$$E_r^{sc}(r, \Delta z) = \frac{Q}{2\varepsilon_0(2\pi)^{3/2}\sigma_0^2\sigma_z} r \int_0^\infty d\zeta \frac{e^{-\frac{1}{2}\left[\frac{r^2}{\sigma_0^2(1+\zeta)} + \frac{\Delta z^2}{\sigma_z^2(1+A^2\zeta)}\right]}}{(1+\zeta)^2\sqrt{(1+A^2\zeta)}} \tag{16}$$

where A is the bunch aspect ratio $A \equiv \sigma_0/\sigma_z$.[21] Since we are interested to rms quantities, we must average over r and Δz in order to compute σ_{pr}^{sc}, the rms transverse space charge momentum:

$$\sigma_{pr}^{sc} = \sqrt{\langle (p_r^{sc})^2 \rangle / 2} = \frac{\pi}{2E_0 \sin\varphi_0} \left[\frac{1}{2Q} \iiint_{V_\infty} \rho(r, \Delta z) E_r^2(r, \Delta z) r dr d\phi dz \right]^{1/2} \tag{17}$$

After substituting Eq. 16 into Eq. 17, finally we get

$$\sigma_{pr}^{sc} = \frac{Z_0 I \cdot \xi(A)}{8E_0 \sin\varphi_0 \cdot \sigma_0} \tag{18}$$

where $Z_0 = 377$ ohm, I is the bunch peak current, $I \equiv Qc/(\sqrt{2\pi}\sigma_z)$, and $\xi(A)$ is a space charge form factor term given by

$$\xi(A) = \left\{ \int_0^\infty d\zeta_1 \int_0^\infty d\zeta_2 \frac{\left[(1+A^2\zeta_1)(1+A^2\zeta_2) + 2 + A^2(\zeta_1+\zeta_2)\right]^{-1/2}}{\left[(1+\zeta_1)(1+\zeta_2) + 2 + \zeta_1 + \zeta_2\right]^2} \right\}^{\frac{1}{2}} \tag{19}$$

As far as a standard bunch aspect ratio is assumed, we found that $\xi(A)$ can be quite well represented by the function

$$\xi(A) = \frac{1}{2.45 + 1.82A^{5/4} - 0.55A^{3/2}} \tag{20}$$

which is accurate within 1% in the range $0 \leq A \leq 6$ (i.e. only exotic pancake bunches at high aspect ratio need to adopt the exact expression in Eq. 19).

According to basic assumptions adopted to calculate the effect of the space charge forces, we will add the contribution of this effect onto the beam envelope behavior simply by assuming that σ_{pr}^{sc} is just a transient rms kick applied to the beam close to the cathode surface: in this respect the space charge contribution is treated in the same manner as the first order RF transverse momentum (p_r^I, Eq. 6).

The total rms transverse momentum σ_{pr}^T at the exit of the second cell ($z = z_{sc}$) will be therefore given just by the superposition of two terms: the RF contribution σ_{pr} given in Eq. 13 and σ_{pr}^{sc}. The effect of σ_{pr}^{sc} on the rms beam size is calculated following the same approach[22] as for Eq. 7: in fact, as for the RF transverse kick p_r^I, we can imagine that the space charge kick σ_{pr}^{sc} is adiabatically transferred from the field to the particle, so that an approximation to the envelope will be $\sigma_r^T = \sigma_r + \frac{1}{z}\int_0^z \frac{z'\sigma_{pr}^{sc}}{\gamma} dz'$. Finally, recalling Eq. 12′ for σ_r, we find

$$\sigma_{pr}^T = \sigma_{pr} + \sigma_{pr}^{sc} \tag{21}$$

$$\sigma_r^T = \sigma_0(1 + \mu\hat{\delta}_2) + \frac{\sigma_{pr}^{sc}}{\alpha k}\hat{\delta}_2 \tag{21'}$$

where σ_r^T is the beam rms size at $z = z_{sc}$.

Since the beam is usually relativistic at the exit of the second cell, the transport matrix[15]

$$M^{RF} \equiv \begin{bmatrix} m_{11} & m_{12} \\ m_{21} & m_{22} \end{bmatrix}$$

$$= \begin{bmatrix} \cos\chi - \sqrt{\frac{2}{\eta}}\sin < \varphi > \sin\chi & \sqrt{\frac{8}{\eta}}\frac{\tilde{\gamma}_2}{\alpha k}\sin\chi \\ \frac{-\eta/2 + \sin^2 < \varphi >}{\sqrt{2\eta}}\frac{\alpha k}{\tilde{\gamma}}\sin\chi & \frac{\tilde{\gamma}_2}{\tilde{\gamma}}\left(\cos\chi + \sqrt{\frac{2}{\eta}}\sin < \varphi > \sin\chi\right) \end{bmatrix},$$

where $\chi \equiv \sqrt{\frac{\eta}{8}}\frac{\log(\tilde{\gamma}/\tilde{\gamma}_2)}{\sin < \varphi >}$, can be used to track the beam envelope throughout the following cells of the photo-injector cavity. The rms beam size σ_{out} at any position z through the cavity is given by

$$\sigma_{out} \equiv \sqrt{(m_{11}\sigma_r^T)^2 + 2m_{11}m_{12}\sqrt{(\sigma_r^T\sigma_r')^2 - \varepsilon^2} + (m_{12}\sigma_r')^2} \tag{22}$$

where $\sigma_r' \equiv \sigma_{pr}^T/\tilde{\gamma}_2$ is the rms beam divergence at the exit of the second cell, and ε is the transverse emittance ($\tilde{\gamma} \equiv 1 + \alpha(kz)\sin < \varphi > + \alpha\cos < \varphi >$ and $\tilde{\gamma}_2 \equiv 1 + (3/2)\pi\alpha\sin < \varphi > + \alpha\cos < \varphi >$).

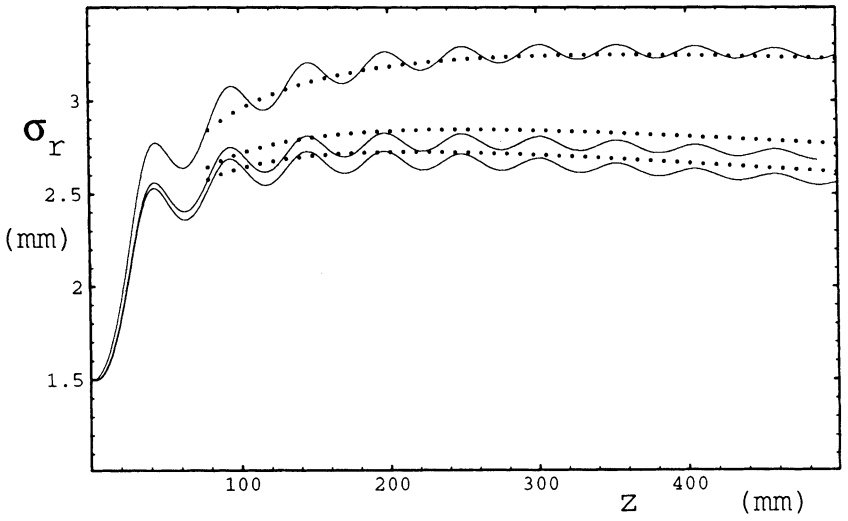

FIGURE 12: Rms beam envelope σ_r plotted as a function of z along a multi-cell RF injector at ν_{RF} = 2.856 GHz, E_0 = 100 MV/m, with a bunch of σ_0 = 1.5 mm, σ_φ = 3.4°RF (3.3 ps), $<\varphi>$ = $\pi/2$ and different charges: 0 nC (no space charge effects, bottom line), 1 nC (central line), 4 nC (top line). Solid line are PIC numerical simulations, dotted lines are analytical predictions on the average beam envelope based on the photocathode starting conditions (see text).

In this way we can predict analytically the beam envelope behavior through the injector just on the basis of the starting conditions at the cathode: the bunch parameters Q, σ_0, σ_φ, $< \varphi >$ and the RF field characteristics α, μ, η.

A comparison between the analytical prediction of Eq. 22 and some numerical results is shown in Figure 12. The RF frequency and field are 2.856 GHz and 100 MV/m, respectively, ($\mu = \eta = 1$), while the bunch starting conditions at the cathode are $\sigma_0 = 1.5$ mm, $\sigma_\varphi = 3.4$°RF (3.3 ps), $< \varphi >= \pi/2$ and charge $Q = 0$ nC for the bottom line, $Q = 1$ nC for the central line, $Q = 4$ nC for the top line. The dotted lines start at the exit of the second cell ($z = 79$ mm) where the analytical values for σ_r^T and σ_{pr}^T are given by Eq. 12, 13, 18, 21, then they follow Eq. 22, which gives, we remind, the averaged (secular) component of the trajectory over the cell-to-cell oscillations. The agreement between numerical data (solid line) and analytical predictions, which are meaningful only at any cell exit, is within a few percent all over the range of charges and positions. It is interesting to note the severe defocusing effect produced by the space charge force at the highest charge level ($Q = 4$ nC).

It should be noticed that the beam envelope transport through the cavity performed by means of Eq. 22 is valid up to the cavity exit: in order to obtain the correct rms beam divergence at the exit we must apply the thin lens matrix

$$\begin{bmatrix} 1 & 0 \\ \frac{\alpha k}{2\tilde{\gamma}_f} \sin < \varphi > & 1 \end{bmatrix}$$

which corresponds to the transient kick[15] applied at the traversal of the cavity exit onto the average component of the trajectory ($\tilde{\gamma}_f$ is the energy at the cavity exit).

4 SUMMARY OF THE FORMULAE

We summarize here the most relevant formulae in order to provide a comprehensive table of scaling laws useful for practical applications.

Formulae concerning rms quantities (σ_r, σ_{pr}) due to RF effects have been re-written adding the dependence on $< \varphi >$: in the previous analysis all the related expression (Eq. 12′ and 13) were intended to be valid at $< \varphi >= \pi/2$. We found that these formulae are approximately valid also for average bunch phases $<\varphi>$ slightly shifted from $\pi/2$ (the error is $O([< \varphi > -\pi/2]^2)$).

In the expressions of the minimum emittance growth ε_x and the rms beam divergence σ_r' we replaced exact but complicated analytical expressions with their corresponding fits on the parameters α, μ, η: these are accurate within 5% over the range $\{0.5<\alpha<6,\ 0.7<\mu<1.3,\ 0.5<\eta<1.5\}$, which covers the usual operating range of RF photo-injectors.

1. RF field parameters α, μ, η:

$$\alpha \equiv \frac{eE_0}{2mc^2k},\ \mu \equiv \sum_{n=1}^{\infty} a_n,\ \eta \equiv \sum_{n=1}^{\infty}(a_{n-1}^2 + a_{n+1}^2 - 2a_{n-1}a_{n+1}\cos(2 < \phi >))$$

$$(a_0 \equiv 0, a_1 \equiv 1)$$

2. Injection phase $<\varphi_0>$ versus exit phase $<\varphi>$:

$$< \varphi_0 >=< \varphi > - \frac{1}{2(\mu\alpha)\sin < \varphi >} - \frac{1}{10(\mu\alpha)^2 \sin^2 < \varphi >}$$

3. Energy gain $\tilde{\gamma}_2$ at the exit of the second cell ($z = 3\lambda/4$):

$$\tilde{\gamma}_2 = 1 + (3/2)\pi\alpha \sin < \varphi > + \alpha \cos < \varphi >$$

4. Bunch parameters at the cathode: $Q, \sigma_0, \sigma_\varphi = k\sigma_z, I = Qc/(\sqrt{2\pi}\sigma_z)$

5. Rms beam size σ_r^T at the exit of the second cell:

$$\sigma_r^T = \sigma_0 \left\{ 1 + (\mu + \mu_{sc}) \left[1 - \frac{(1 + \alpha \cos < \varphi >) \log \tilde{\gamma}_2}{\tilde{\gamma}_2 - 1} \right] \right\},$$

$$\mu_{sc} = \frac{Z_0 I \xi(A)}{8(\alpha k) E_0 \sin < \varphi_0 > \sigma_0^2}$$

$$\xi(A) = \frac{1}{2.45 + 1.82A^{5/4} - 0.55A^{3/2}}$$

6. Rms beam divergence at the exit of the second cell:

$$\sigma_r' = \frac{\alpha k \sigma_0}{\tilde{\gamma}_2}\left[\left(\tilde{p}_r + \Psi \cdot \sigma_\varphi^2\right)\sin < \varphi > + \mu_{sc}\right],$$

$$\tilde{p}_r = \left\{\mu\left[1 + \mu - \frac{\mu \log \gamma_1^*}{\gamma_1^* - 1}\right] - \frac{\delta\eta \log \gamma_2^*}{8 \sin^2 < \varphi >}\left[1 + \mu - \frac{\mu \log\left(\gamma_1^* \sqrt[3]{\gamma_2^*}\right)}{2(\gamma_1^* - 1)}\right]\right\}$$

$$\gamma_2^* = \tilde{\gamma}_2 - \alpha \cos < \varphi >, \quad \gamma_1^* = 1 + (1/2)\pi\alpha \sin < \varphi >, \int = 1 - \left(\frac{\alpha}{4!}\right)^2$$

$$\Psi = \frac{\alpha^2}{578}(\eta^2 + 8.3\mu^2) - \frac{\alpha}{34}(\eta^2 + 5\mu^2) - \frac{\mu}{11}(6.3 + 0.15\eta + \mu)$$

7. Rms normalized transverse emittance growth ε_x from RF effects:

$$\varepsilon_x = \left(\frac{\alpha}{\sqrt{2}} k \sigma_0^2 \sigma_\varphi^2\right) \bullet$$

$$\left\{(\alpha/9)^2[0.72\mu - \mu(\eta - 5\mu)] - \frac{\alpha}{29}(\eta^2 + 18\mu^2) + 1.3\mu\left(\frac{1}{2} - \mu - \frac{\eta}{11}\right) - 0.54\right\}$$

5 CONCLUSIONS

We have shown that it is possible to predict analytically the behavior of the radial beam envelope inside a photo injector cavity just on the basis of the beam starting conditions at the cathode and of the RF field characteristics: these are the bunch charge, radial size and length and the RF field frequency, gradient and higher spatial harmonic content.

The analytical formulae agree quite remarkably with numerical data generated by sophisticated multi-particle codes (which, in turn, have been extensively checked in the past against experimental measurements). This holds in a broad range of beam and RF field parameters, covering most of the existing and planned RF photo injectors.

The approach to beam dynamics analysis here presented is applicable whenever charged particles are generated at rest in presence of very intense em. fields, capable to bring them up to relativistic velocities in a distance shorter than the wavelength.

REFERENCES

1. J.S. Fraser *et al.*, IEEE Trans. Nucl. Sci. NS-32 (1985), p. 1791; R.L. Sheffield *et al.*, Proc. 1988 Linear Accelerator Conf., Williamsburg, VA, Oct. 1988, CEBAF rep. 89–001 (1989), p. 520.
2. C. Travier, Particle Accelerators 36 (1991), p. 33.
3. K.J. Kim, NIM A275 (1989), p. 201.
4. B.E. Carlsten, IEEE Catalog no. 89CH2669–0 (1989) p. 313; B.E. Carlsten and R.L. Sheffield, Proc. 1988 Linear Accelerator Conf., Williamsburg, VA, Oct. 1988, CEBAF rep. 89–001 (1989), p. 365.

5. J.C. Gallardo and R.B. Palmer, NIM A304 (1991), p. 345.
6. J. Gao, NIM A304 (1991), p. 348; J. Gao, NIM A304 (1991), p. 353.
7. L. Serafini *et al.*, NIM A318 (1992), p. 301; L. Serafini *et al.*, INFN rep. INFN/TC-91/07 (1991).
8. J.B. Rosenzweig and J. Smolin, AIP Conf. Proc. 279 (1993), p. 684.
9. L. Serafini, AIP Conf. Proc. 279 (1993), p. 645.
10. C. Travier, NIM A340 (1994), p. 26.
11. L. Serafini, NIM A340 (1994), p. 40.
12. J.M. Dolique and J.C. Coacolo, IEEE Catalog no. 91CH3038–7 (1991), p. 233; J.M. Dolique and J.C. Coacolo, NIM A340 (1994), p. 231.
13. L. Serafini, NIM A341 (1994), p. 341.
14. J.C. Gallardo and H.G. Kirk, IEEE Catalog no. 93CH3279–7 (1993), p. 3615.
15. J.B. Rosenzweig and L. Serafini, Phys. Rev. E-**49** (1994), p. 1599.
S.C. Hartman and J.B. Rosenzweig, Phys. Rev. E-**47** (1993), p. 2031.
16. W.K.H. Panofsky and W.A. Wenzel, Rev. Sci. Instr. 27 (1956), p. 967.
17. Note that higher spatial harmonics give actually no net contribution to the energy gain when averaged over one cell: since they have usually a small amplitude with respect to the fundamental one, we will neglect here also the weak oscillations induced in the behavior of the energy gain versus z.
18. K.T. McDonald, "Design of the laser-driven Radio-Frequency electron Gun for the Brookhaven Accelerator Test Facility", Princeton University int. rep., January 17, 1988.
K. Batchelor, H. Kirk, J. Sheehan, M. Woodle, K. McDonald, Proc. 1st EPAC, Rome, June 1988, Ed. World Scientific, p. 954.
19. L. Serafini and C. Pagani, Proc. 1st EPAC, Rome, June 1988, Ed. World Scientific, p. 866.
20. E. Keil, IEEE Catalog no. 87CH2387–9 (1987), p. 1319.
21. Here φ_0 must be intended as the average bunch injection phase at the cathode, i.e. the phase at which the laser pulse center strikes the cathode surface.
22. We can apply the results found on the particle trajectory straightly on the beam envelope since the beam is actually a quasi-laminar beam: its temperature emittance is usually quite small so that in the envelope equation[23] the emittance term is negligible[15].
23. J.D. Lawson, *The Physics of Charged Particle Beams*, 2nd ed. (Oxford University Press, New York, 1988).